J. Appl. Comput. Mech., 7(2) (2021) 528-534
DOI: 10.22055/JACM.2020.35159.2583

ISSN: 2383-4536
jacm.scu.ac.ir

Shahid Chamran University of Ahvaz

Journal of Applied and Computational Mechanics

Research Paper

Computational Study of Flow around 2D and 3D Tandem Bluff Bodies

Terrance Charles, Zhiyin Yang, Yiling Lu

School of Computing and Engineering, College of Science and Engineering, University of Derby, Derby, UK

Received September 25 2020; Revised October 29 2020; Accepted for publication October 29 2020.
Corresponding author: Zhiyin Yang (z.yang@derby.ac.uk)

Abstract. Numerical simulations have been carried out to advance our current understanding of flow around two dimensional (2D) and three dimensional (3D) square shaped tandem bluff bodies at a Reynolds number of 22,000, especially to shed light on the sudden change of the downstream body's drag coefficient. The Reynolds-Averaged Navier-Stokes (RANS) approach has been employed in the present study and the predicted drag coefficients compare reasonably well with available experimental data. Better understanding of flow fields has been achieved by analyzing streamlines, velocity vectors for both 2D and 3D cases in a horizontal plane and a vertical symmetric plane. The sudden jump in drag coefficient of the downstream body for the 2D case is well captured numerically, which is due to the flow over the upstream body impinging onto the front face of the downstream body at a critical gap size between those two bodies. For the 3D case the drag coefficient is predicted to increase gradually, consistent with the previous experimental finding. This is due to the fact that the vortical structures formed in the 3D case are very different, resulting in a reasonably smooth change of the flow field around the upstream body and hence leading to a gradual, not sudden, increase in the drag coefficient of the downstream body.

Keywords: Tandem bluff bodies, Drag coefficient, RANS, Numerical simulation.

1. Introduction

The aerodynamic study of the flow field around bluff bodies has been a subject of immense interest since it has a practical significance in many different engineering disciplines such as Civil Engineering and Automotive Engineering. Studies in this area have increased in the last few decades due to their simple geometry but practical and realistic significance such as aerodynamics drag reduction of trucks [1-2].

An important feature of bluff body flow is the flow separation where the location of separation may strongly affect the aerodynamic characteristic of the body. The most used bluff body shapes are (a) circular cylinder and (b) square cylinder. The arrangement of these bluff bodies can range from tandem to staggered arrangement. Experiments have been conducted with side to side arrangement, perpendicular and parallel to the incoming flow for 2D and 3D bodies. A 2D bluff body extends a long way (theoretically, it should be infinitely) in the spanwise direction. While a 3D bluff body is the case with a finite length in the spanwise direction and hence its end effects play an important role, leading to very different flow field around the bluff body.

Previous studies around 2D bluff bodies have concentrated on circular cylinders in a tandem arrangement. Experiments carried out by Zdravkovich [3] provide extensive information for twin circular cylinders in various arrangements (tandem, side by side and staggered). The author demonstrated that for the tandem arrangement there existed very complex flow fields and different interference regimes. In particular, there was a discontinuous change of the pressure on the front face of the downstream cylinder against the gap spacing between the two cylinders. Similar flow patterns have been identified by Zhang and Melbourne [4] for circular cylinders, Hangan and Vickery [5] for square cylinders in a tandem arrangement.

The flow around 3D rectangular bluff bodies has been studied due to their practical applications [6-8]. Flow field around 3D tandem bluff bodies consist of very complex characteristics with the formation of streamwise and spanwise vortices which interact with each other. The vortices formed at the rear of the obstacle tend to change the flow fields and the downstream recovery of the flow.

Numerous previous studies have been done on flow around two tandem circular cylinders and relatively little attention has been focused on flow over two tandem square cylinders. Several previous studies on square cylinders have demonstrated that the gap spacing between the two tandem cylinders has a great impact on the flow field around the cylinders. Some dramatic changes of flow pattern occur at a critical spacing [9-14], leading to the surface pressure, drag coefficient, and vortex-shedding frequency being altered rapidly around the critical spacing. In particular, it has been found that when the gap spacing is bigger than the critical spacing a sudden significant increase in the drag force occurs to the downstream cylinder. This sudden increase is very sharp in the 2D flow case while in the 3D flow case the drag force increases gradually. However, the mechanisms behind the sharp increase in the 2D case and the gradual increase in the 3D case is not fully understood and the main objective of the present study is to advance our current understanding in this area through a detailed numerical study of 2D and 3D flows around tandem bluff bodies.

Published online: November 21 2020

2. Mathematical Formulation and Numerical Procedure

2.1 Governing equations

The governing equations are derived from conservation laws for mass and momentum, which are three dimensional and time-dependent for turbulent flow. The Reynolds-Averaged Navier-Stokes (RANS) approach for computing turbulent flow is employed in the present study. The RANS equations are obtained by time-averaging the instantaneous governing equations. This averaging process leads to extra terms called Reynolds stresses which need to be approximated by a turbulence model.

The flow is treated as isothermal and incompressible in the present study since there is no heat transfer and air velocity is very low. The RANS equations for incompressible flow are fairly standard and are given in many textbooks and papers [15-18], and hence will be presented very briefly here.

Continuity equation:

$$\frac{\partial \bar{U}_i}{\partial x_i} = 0 \tag{1}$$

Momentum equation:

$$\frac{\partial \bar{U}_i \bar{U}_j}{\partial x_i} = -\frac{1}{\rho}\frac{\partial \bar{P}}{\partial x_i} + \frac{\partial}{\partial x_i}\left[\nu \frac{\partial \bar{U}_j}{\partial x_i}\right] - \frac{\partial\left(\overline{u_i' u_j'}\right)}{\partial x_i} \tag{2}$$

The last term on the right hand of the above momentum equation is the Reynolds stress term and needs to be modelled (approximated) by a turbulence model. Numerous turbulence models are available but there is no general agreement that which model is the best as their performances vary depending on flow situations. In the present study, the realizable k–ε turbulence model is chosen since this turbulence model can predict complex flow features such as separation, re-circulation etc. better than the standard k–ε model and other two equation turbulence models. The more advanced turbulence models based on Reynolds stress transport equations, called Reynolds Stress Model (RSM), have been developed. But it is very expensive computationally as six additional transport equations need to be solved, and especially in many flow cases a RSM does not show superiority over two equations turbulence models. Two other more accurate approaches for simulating turbulent flow, Direct Numerical Simulation and Large-Eddy Simulation, are still far too computationally expensive [20-21] for practical engineering flow problems.

The governing equations are solved numerically using a finite volume method. A pressure-based approach is selected since the flow is treated as incompressible. The computer code used is STAR CCM+ and the second-order upwind scheme is employed for spatial discretization.

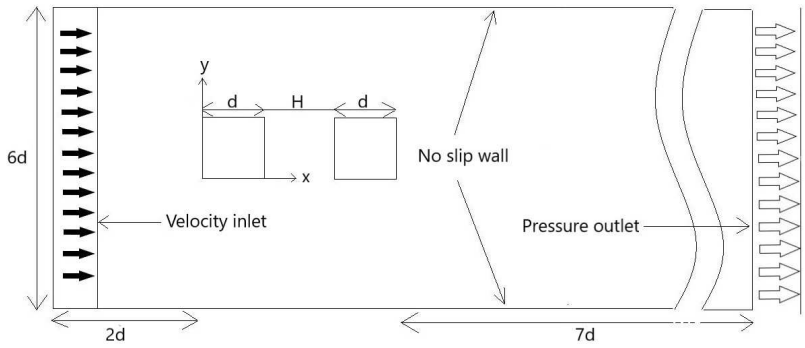

Fig. 1. Computational domain for 2D simulations.

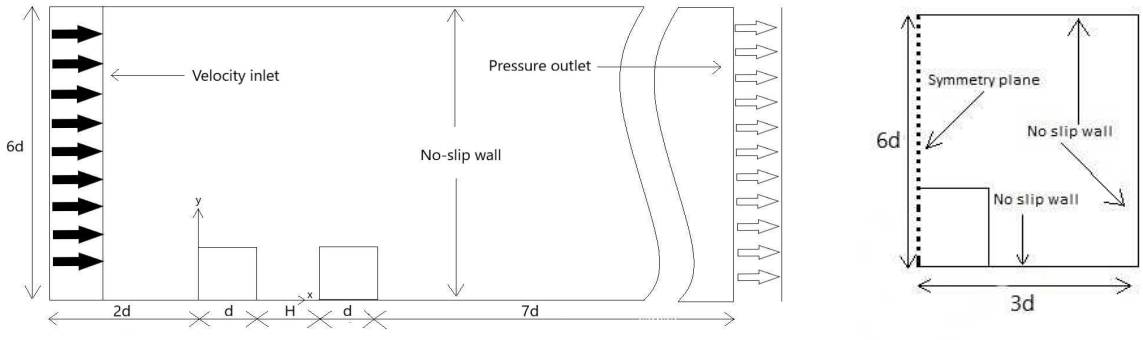

(a) (b)

Fig. 2. Computational domain for 3D simulations. (a) Side view of the domain, (b) From view of the domain.

2.2 Computational details

The computational domain adopted for simulations of 2D flow past tandem square cylinders is shown in Figure 1, which has an upstream length of 2d (d = 40 mm, the height of the square), a downstream length of 7d from the back face of the downstream cylinder and a height of 6d. A uniform velocity of 8.0 m/s is specified at the inlet, corresponding to a Reynolds number of 22,000 based on the square height, matching the value in the experiment [6]. Inlet turbulent intensity is specified as 1.5% based on the experimental data. A pressure outlet boundary condition is applied at the outflow boundary. A no-slip wall boundary condition is applied at the top/bottom walls and cylinder surfaces.

The computational domain for the 3D flow simulations is the same as the computational domain for the 2D flow case apart from that the width of the domain is 6d. Two identical cubes with the same size of d as in the 2D case are placed on the bottom of the domain as shown in Figure 2. The same boundary conditions used in the 2D case are applied in the 3D case and a no-slip boundary condition is applied at the side walls. In order to save computational cost the computational domain is cut at z = 0 into two domains and only half of the original domain is used in the simulation with a symmetry boundary condition being applied on the cut plane at z = 0 as shown in Figure 2b.

3. Results and Discussion

The CFD model used in the present study has already been validated in the author's previous work [8] with a good agreement between the predictions and the experimental data (velocity profile and drag coefficient). Hence there is no need to present those results again here and the rest of this section will be devoted to advancing our current knowledge on the mechanisms behind the sharp increase of the downstream bluff body drag force in the 2D case and the gradual increase in the 3D case.

3.1 Two-dimensional flow case

3.1.1 Drag coefficient

Figure 3 presents the predicted drag coefficient and the experimental data of the downstream cylinder [5, 19] against the non-dimensional gap spacing (H/d) for the 2D case. Both the prediction and experimental data show a sharp increase in the drag coefficient when the gap spacing is bigger than a "critical gap spacing". The critical gap spacing depends on many factors such as Reynolds number, turbulent intensity of the incoming flow etc. Hence it is not surprising to see that the predicted critical spacing in the present study is around H/d = 1.7 while the measured value by Ricciardeli [19] is about H/d = 1.45 and the data by Hangan & Vickery [5] shows much larger at about H/d = 1.95. This sudden increase of the downstream cylinder drag at a critical gap spacing has also been reported in many previous studies and detailed analysis will be presented below to reveal the change of the flow fields when the gap spacing changes, leading to a better understanding of the drag coefficient variations observed in Fig. 3.

3.1.2 Flow field

Figure 4 shows the mean velocity vectors and streamlines around 2D tandem square cylinders at a gap spacing of H/d = 1 which is below the predicted critical spacing of 1.7. Figure 3 shows that the flow field is very complicated with flow separation occurring at several locations and a few recirculation regions forming around two cylinders. One distinct feature is that the flow on the top and bottom are not symmetric at all. It can be seen more clearly from Fig. 4b that a large vortex (V1) appears on top of the upstream cylinder while a much smaller vortex (V2), about half size of V1, forms at the bottom. The flow around the downstream cylinder is even more asymmetric since there exists a separation eddy (V3) near the leading edge of the bottom surface while no such a separation eddy forms near the leading edge of the top surface at all. In the wake region behind the downstream cylinder a single large recirculation region (V4) is clearly observable. It is very important to note that a large portion of the flow over the top of the cylinder enters the gap region almost vertically without impinging onto the front face of the downstream cylinder at all. This means that there are no high pressure regions formed on the front face of the downstream cylinder, resulting in low pressure drag force of the downstream cylinder at this gap spacing. Actually as shown in Fig. 3 that at this gap spacing (H/d = 1) the drag coefficient is negative and this is because the pressure force on the back face of the downstream cylinder is slightly larger than the pressure force on the front face of the cylinder.

The flow filed is quite different when the gap spacing increases to H/d = 2, above the critical spacing of 1.7 as shown in Figure 5 that the flow becomes more asymmetric apart from the flow on top and bottom of the upstream cylinder where reasonably two similar separation vortices (V1 & V2) appear at the top and bottom of the tractor. Significant change can be observed behind the upstream cylinder with a large vortex formed in the gap region (V3) as shown in Fig. 5b. The flow in the gap region is mainly from top of the upstream cylinder, which impinges obliquely onto the front face of the downstream cube, resulting in high pressure on this surface and this is why the pressure coefficient for the downstream cylinder increases rapidly from a negative value to a positive value as shown in Fig. 3. The flow filed on top of the downstream cylinder is totally different from that at the bottom as shown in Fig. 5b, and also the vortex formed at the back of the downstream cube (V5) becomes smaller compared with the case at H/d = 1.

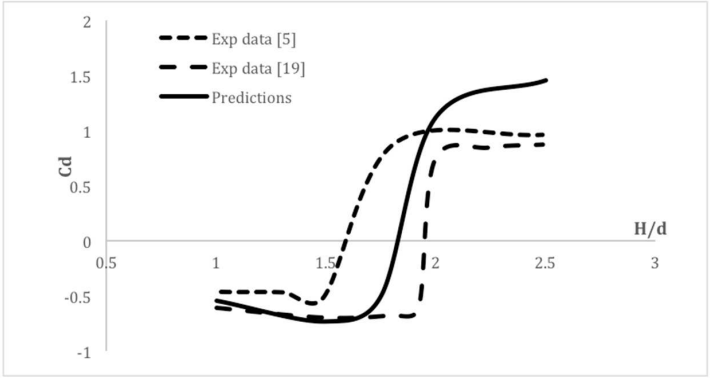

Fig. 3. Variations of the downstream cylinder pressure coefficient against the non-dimensional gap spacing.

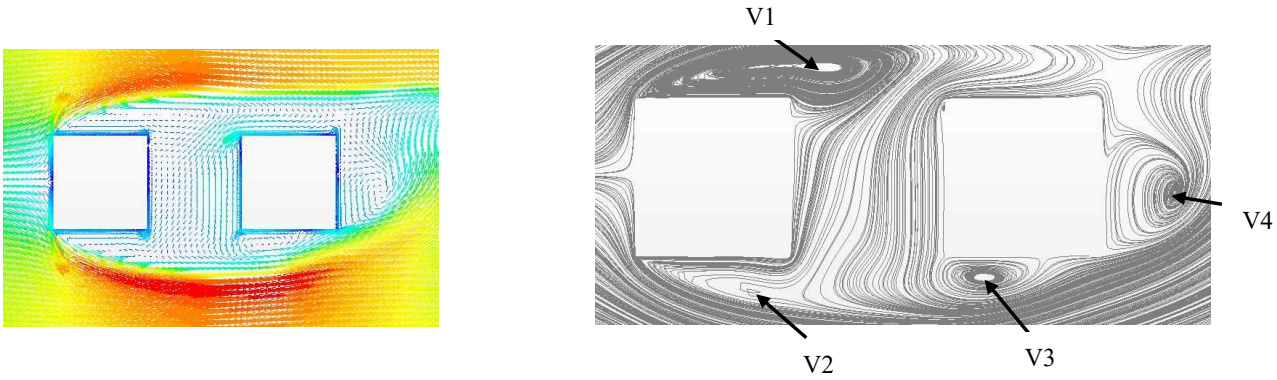

Fig. 4. 2D flow field around two tandem square cylinders at H/d = 1: (a) velocity vector plot, (b) streamline plot.

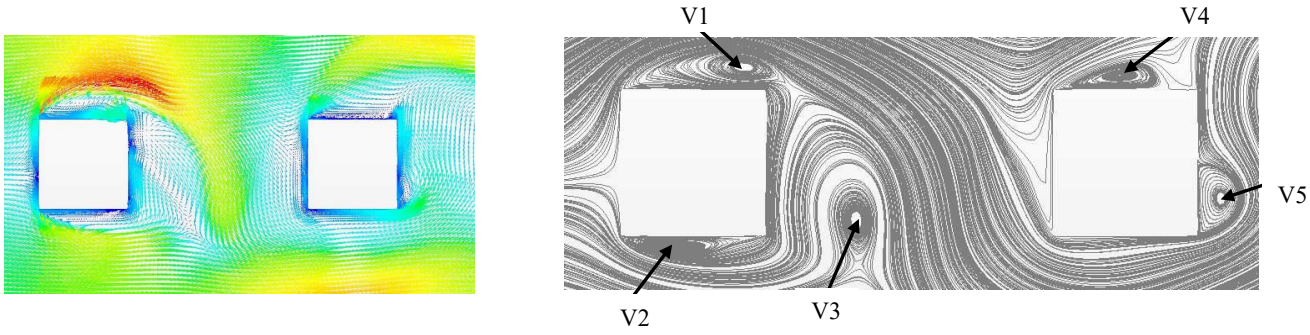

Fig. 5. 2D flow field around two tandem cylindrs at H/d = 2: (a) velocity vector plot, (b) streamline plot.

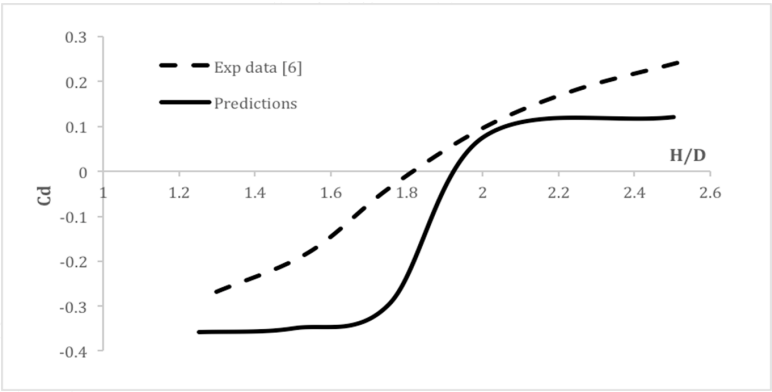

Fig. 6. Change of the downstream cylinder pressure coefficient with the non-dimensional gap spacing.

3.2 Three-dimensional flow case

3.2.1 Drag coefficient

Figure 6 plots the predicted and measured drag coefficient of the downstream cube against the dimensionless gap spacing (H/d) for the 3D case. Unlike the 2D case in the previous section, both the prediction and experimental data show that there is no sudden increase of the drag coefficient with the increase of the gap spacing for the 3D case. The predicted drag coefficient starts to increase gradually at about H/d = 1.47 till about H/d = 1.75, and after this a more steep increase occurs till about H/d = 2; while the experimental data show an even more gradual increase starting from about H/d = 1.3 and still keep on increasing slowly after H/d = 2. Further flow field analysis on the symmetry XY plane and a XZ plane is presented below to have a better understanding of the drag coefficient variations shown in Fig. 6.

3.2.2 Flow field

Figure 7 shows the velocity vectors on the symmetry XY plane at H/d = 0.5 and it can be seen that very complex flow structures are generated. The flow separates at the leading edge of the upstream cube top surface and reattaches to the top surface of the downstream cube forming a single semi-elliptical shaped recirculation region on top of the two cubes. This acts like a single vortex at the top face of both cubes and no strong interaction occurs between this vortex and the flow inside the gap

region. The flow field in the gap region is dominated by a large vortex occupying almost 80% of the total gap region and some small flow structures are formed in the bottom half of the gap region near the wall. Since there is no strong interaction between the flow inside the gap region and the flow outside it, and especially no flow impingement on the front face of the downstream cube, the pressure force on the front face is relatively smaller than the counterpart on the back face, resulting in a negative drag coefficient at this gap spacing as shown in Fig. 6. In the wake region behind the second cube, a typical vortex is observed which is commonly reported in flows over a single cube and a backward facing step.

Figure 8 shows velocity vectors on the symmetry XY plane at three gap sizes (H/d = 0.25, 0.75, 1 and 2) and in the case at H/D = 0.25, the primary recirculation zone on top of the two cubes and the flow field in the wake of the second cube resemble those at H/d = 0.5 as shown in Figure 7. However, the flow field in the gap region is quite different from the case at H/d = 0.5 as the flow field is no longer dominated by a single large vortex by some smaller but quite complex flow structures (see Figure 8a). Similar to the case at H/D = 0.5 there is no flow impingement on the front face of the second cube and hence the drag coefficient is also negative as discussed above.

For the case at H/d = 0.75, the single semi-elliptical shaped recirculation region on top of the two cubes observed at H/d = 0.25 and 0.5 is still just about observable as shown in Figure 8b and is in the brink of breaking into two recirculation zones. It can be also seen that there is more interaction between the flow inside the gap region and the flow outside it. The flow field in the gap region becomes more complex, which is also not dominated by a large single vortex. The flow field in the wake region behind the second cube is similar to that in previous cases. The drag coefficient remains negative as the total pressure force on the front face of the second cube is still lower than the counterpart on the back face.

When the gap size increases to H/d = 1.0, the single semi-elliptical shaped recirculation region on top of the two cubes observed in the previous cases breaks into two recirculation regions as shown in Figure 8c, leading to a much stronger interaction between the flow above the cubes and the flow inside the gap region with more flow entering the gap region. However, the flow entering the gap region does not impinge on the front face of the second cube and hence the pressure force on the front face is still smaller than that on the back face, keeping the drag coefficient to a negative value. The gross flow field in the wake region behind the second cube is more or less the same as those in the previous three cases.

As the gap size increases further to H/D = 2.0, the single and two semi-elliptical shaped recirculation regions on top of the two cubes observed in the previous three cases disappear completely as shown in Figure 8d. Furthermore, a large proportion of flow past the upstream cube enters the gap region and impinges on the front face of the downstream cube, resulting in a large increase in pressure on this surface and hence leading to a significant increase of the drag coefficient as shown in Figure 6.

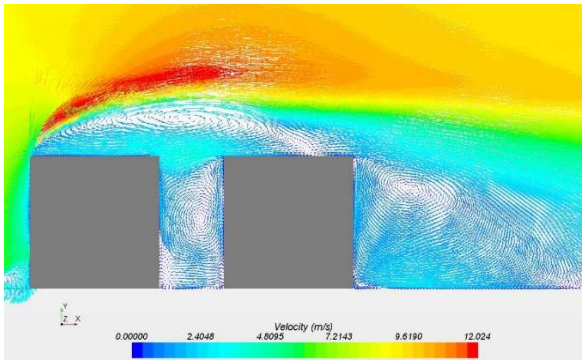

Fig. 7. Velocity vectors on the symmetry XY plane at H/d = 0.5.

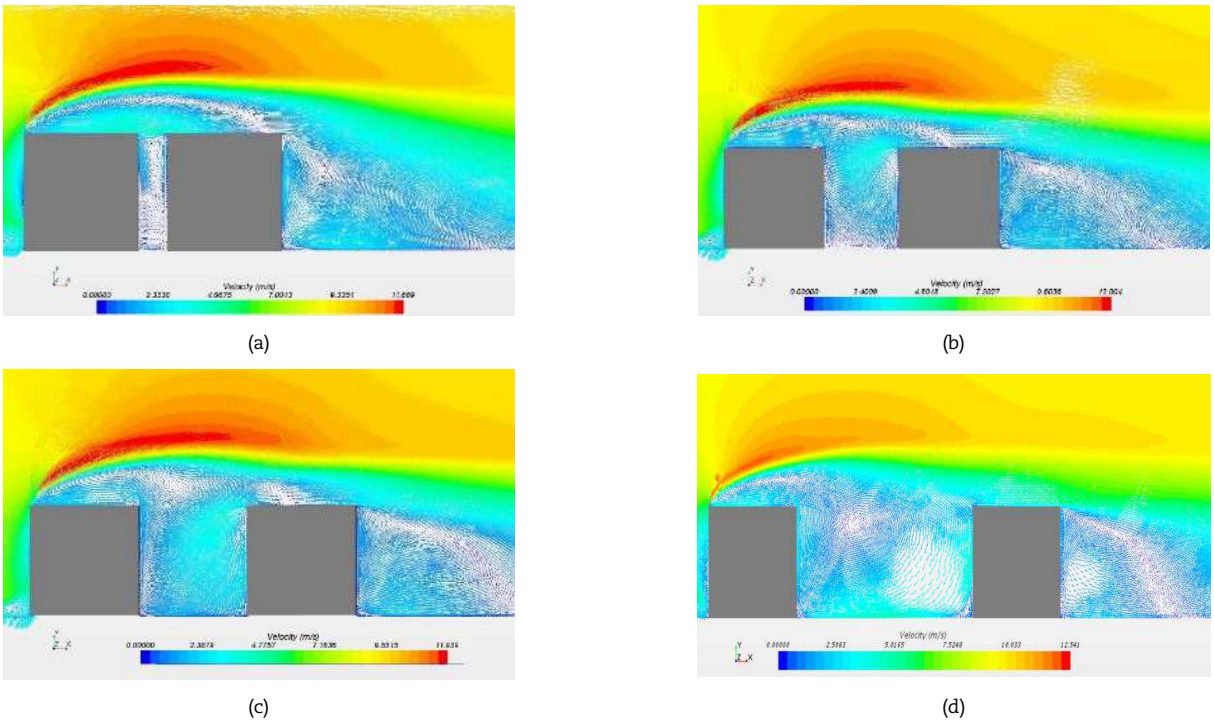

(a) (b)

(c) (d)

Fig. 8. Velocity vectors on the symmetry XY plane at different gap sizes H/d = 0.25 (a), 0.75 (b), 1.0 (c), 2.0 (d).

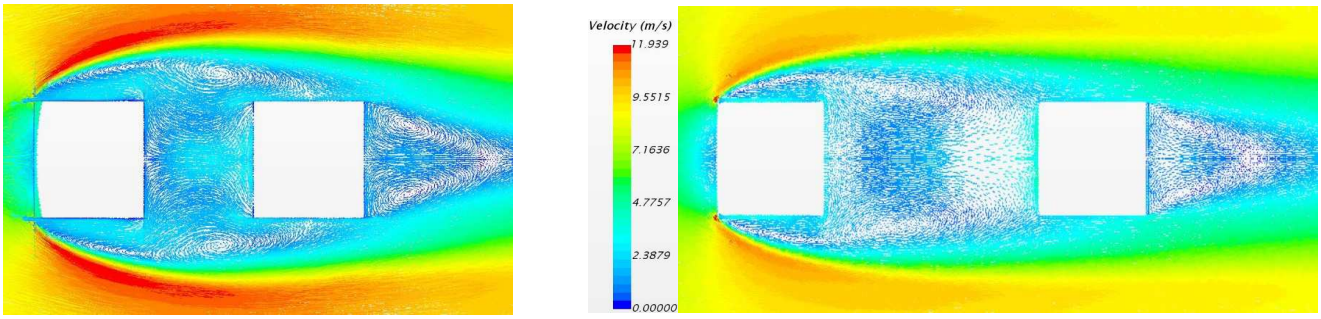

Fig. 9. Velocity vectors on a XZ plane at H/d = 1 (a), 2 (b).

Figure 9 presents the velocity vectors around the 3D tandem cubes on the horizontal XZ plane (at Y/d = 0.5) for cases of H/d = 1 and 2. One distinct flow feature at H/d = 1 shown in Figure 9a is that the flow separates at the leading edge of the upstream cube lateral surfaces and reattaches to the lateral surfaces of the downstream cube forming a single semi-elliptical shaped recirculation region on both sides of the two cubes. This is similar to the flow feature observed on the XY plane as shown in Figures 7 and 8a-b. In particular, the formation of this single semi-elliptical shaped recirculation region prevents flow past the lateral side impinging directly on the front face of the downstream cube at this gap spacing of H/d = 1. This confirms the above analysis based on Figures 7 and 8 that the pressure force on the front face of the downstream cube is relatively smaller than the pressure force on the back face, leading to a negative drag coefficient at this gap spacing as shown in Figure 6. However, at H/d = 2 the flow separating at the leading edge of the upstream cube lateral surfaces does not reattach to the lateral surfaces of the downstream cube. As a result of this, a certain proportion of flow past the upstream cube lateral sides impinges on the front face of the downstream cube, leading to a large increase in pressure on this surface. This confirms the analysis based on Figures 7 and 8 why there is a significant increase of the drag coefficient when the gap spacing increases as shown in Figure 6.

4. Conclusion

A numerical study of flow around 2D and 3D tandem bluff bodies has been carried out to investigate the influence of the gap spacing on the flow field, especially to improve our current understanding why there is a sudden change of the downstream body drag in the 2D case at a critical gap spacing whereas such change is gradual in the 3D case. The RANS approach has been used in the present study and a reasonably good agreement between the predicted drag coefficients and available experimental data has been obtained. Detailed analysis of the flow field has been performed to understand the mechanism behind the sudden increase of the downstream body drag in the 2D case and the gradual increase in the 3D case with the following new findings:

- For the 2D case when the gap spacing is smaller than a critical spacing the flow over the upstream body does not imping onto the front face of the downstream body, leading to relatively low pressure on the front face of the downstream body which results in a low drag. However, at the critical gap spacing the flow field changes drastically and the flow over the upstream body starts to imping onto the front face of the downstream body, leading to a sudden increase of the pressure on the front face of the downstream body and consequently the sudden increase of the drag.
- For the 3D case flow structures are quite different as flow can go not only over the upstream cube but also around the lateral sides of the cube, resulting in a reasonably gradual change of flow field in the gap region as the gap spacing increases. Therefore, there is no sudden increase of pressure on the front face of the downstream cube at a certain gap spacing, leading to a gradual increase of the drag coefficient.

Author Contributions

Z. Yang planned the project and suggested the simulations; T. Charles conducted the numerical simulations and processed the data; Y. Lu provided help in conducting the simulations. The manuscript was written through the contribution of all authors. All authors discussed the results, reviewed and approved the final version of the manuscript.

Acknowledgments

The research facilities/support provided by the University of Derby is gratefully acknowledged.

Conflict of Interest

The authors declared no potential conflicts of interest with respect to the research, authorship and publication of this article.

Funding

T. Charles's Ph.D. study has been partly funded by the University of Derby.

Nomenclature

2D	Two dimensional	$\overline{U}_i$	Mean velocity component (I = 1, 2, 3)
3D	Three dimensional	x_i	Spatial coordinate (i = 1, 2, 3)
k-ε	*k-ε* turbulence model	ρ	Fluid density
RANS	Reynold Averaged Navier Stokes	$\overline{u}_i'$	Fluctuating velocity component (i = 1, 2, 3)
RSM	Reynolds Stress Model	H	Gap between tractor and trailer

p	Mean fluid pressure	C_d	Drag coefficient
d	Height of the square/cube	υ	Fluid kinematic viscosity

References

[1] Abikan, A., Yang, Z., Lu, Y., Computational Analysis of Turbulent Flow over a Bluff Body with Drag Reduction Devices, *Journal of Applied and Computational Mechanics*, 6(SI), 2020, 1210-1219.
[2] Charles, T., Yang, Z., Lu, Y., Assessment of Drag Reduction Devices Mounted on a Simplified Tractor-Trailer Truck Model, *Journal of Applied and Computational Mechanics*, 6(SI), 2020, 1466-1474.
[3] Zdravkovich, M.M., Review of Flow Interference between Two Circular Cylinders in Various Arrangement, *Journal of Fluids Engineering*, 99, 1977, 618-633.
[4] Zhang, H., Melbourne, W., Interference between Two Circular Cylinders in Tandem in Turbulent Flow, *Journal of Wind Engineering and Industrial Aerodynamics*, 41, 1992, 589-600.
[5] Hangan, H., Vickery, B., Buffeting of Two Dimensional Bluff Bodies, *Journal of Wind Engineering and Industrial Aerodynamics*, 82, 1999, 173-187.
[6] Martinuzzi, R. J., Havel, B., Vortex Shedding of Two Surface Mounted Cubes in Tandem, *International Journal of Heat and Fluid Flow*, 25, 2004, 364-372.
[7] Saïd, N. M., Mhiri, H., Philippe, C., Palec, G. L., Phillippe B., Wind Tunnel Investigation and Numerical Simulation of the Near Wake Dynamics for Rectangular Obstacles, *Environmental Engineering Science*, 25, 2008, 1037-1060.
[8] Charles, T., Lu, Y., Yang Z., Impacts of the Gap Size between Two Bluff Bodies on the Flow Field within the Gap, *Proceedings of the 13th International Conference on Heat Transfer, Fluid Mechanics and Thermodynamics*, 2017, 132-135.
[9] Sakamoto, H., Haniu, H., Obata, Y. Fluctuating Forces Acting on Two Square Prisms in a Tandem Arrangement, *Journal of Wind Engineering and Industrial Aerodynamics*, 26, 1987, 85-103.
[10] Sakamoto, H., Haniu, H., Effect of Free-stream Turbulence on Characteristics of Fluctuating Forces Acting on Two Square Prisms in Tandem Arrangement, *Journal of Fluids Engineering*, 110, 1988, 140-146.
[11]. Luo, S. C., Teng, T. C., Aerodynamic Forces on a Square Section Cylinder That is Downstream to an Identical Cylinder, *The Aeronautical Journal*, 94, 1990, 203-212.
[12] Ljungkrona, L., Norberg, C., Sunden, B. Free-stream Turbulence and Tube Spacing Effects on Surface Pressure Fluctuations for Two Tubes in an In-line Arrangement, *Journal of Fluids and Structures*, 5, 1991, 701-727.
[13] Liu, C., Chen, J. M., Observations of Hysteresis in Flow around Two Square Cylinders in a Tandem Arrangement, *Journal of Wind Engineering and Industrial Aerodynamics*, 90, 2002, 1019-1050.
[14] Kim, M. K., Kim, D. K., Yoon, S. H., Lee, D. H., Measurements of the Flow Fields Around Two Square Cylinders in a Tandem Arrangement, *Journal of Mechanical Science and Technology*, 22, 2008, 397-407.
[15] Worth, N., Yang, Z., Simulation of an Impinging Jet in a Crossflow Using a Reynolds Stress Transport Model, *International Journal of Numerical Method in Fluids*, 52, 2006, 199-211.
[16] Ostheimer, D., Yang, Z., A CFD study of Twin Impinging Jets in a Cross-flow, *The Open Numerical Methods Journal*, 4, 2012, 24-34.
[17] Yang, Z., Assessment of Unsteady-RANS Approach against Steady-RANS Approach for Predicting Twin Impinging Jets in a Cross-flow, *Cogent Engineering*, 1, 2014 936995.
[18] Ostheimer, D., Yang, Z., Numerical Simulation of Twin Impinging Jets in a Cross-flow. *The 3rd International Symposium on Jet Propulsion and Power Engineering*, Nanjing, China, 2010-ISJPPE-1035, 2010.
[19] Ricciardelli, F., *Aerodynamics of a Pair of Square Cylinders*, M.E.Sc. Thesis, The University of Western Ontario, Canada, 1994.
[20] Yang, Z., Large-Eddy Simulation: A Glance at the Past, a Gaze at the Present and a glimpse at the Future, *The 5th International Symposium on Jet Propulsion and Power Engineering*, Beijing, China, 2014-ISJPPE-0010, 2014.
[21] Yang, Z., Large-Eddy Simulation: Past, Present and the Future, *Chinese Journal of Aeronautics*, 28(1), 2015, 11-24.

ORCID iD,

Terrance Charles https://orcid.org/0000-0002-1159-4532
Zhiyin Yang https://orcid.org/0000-0002-6629-1360
Yiling Lu https://orcid.org/0000-0001-6084-5425

How to cite this article: Charles T., Yang, Z., Lu, Y., Computational Study of Flow around 2D and 3D Tandem Bluff Bodies, *J. Appl. Comput. Mech.*, 7(2), 2021, 528–534. https://doi.org/10.22055/JACM.2020.35159.2583